SUPPLEMENTAL FIGURES

Supplemental Fig. S1. Biological processes altered in Mφs by modulation of *Mknk1* and *Mknk2* levels.

(**A–C**) BMDMs were transduced with control shRNA (shCtr), sh*Mknk1* or sh*Mknk2* lentivirus, and treated with or without an MNK inhibitor (MNKi). (**A**) Quantification of total eIF4E protein normalized to β–actin. (**B, C**) qPCR analysis confirming knockdown efficiency of *Mknk1* (**B**) and *Mknk2* (**C**) relative to shCtr–transduced BMDMs. (**D–F**) BMDMs were transduced with empty vector (EV), *Mknk1* or *Mknk2* overexpression lentivirus. (**D**) Quantification of total eIF4E protein normalized to β–actin. (**E, F**) qPCR analysis of *Mknk1* (**E**) or *Mknk2* (**F**) expression relative to EV–transduced BMDMs. (**G–L)** Quantitative proteomics (HiRIEF LC–MS/MS) of BMDMs following MNK silencing (shCtr, sh*Mknk1*, sh*Mknk2*) or MNK overexpression (EV, *Mknk1*, *Mknk2*). (**G, H**) Principal component analysis (PCA) plots showing PC1 versus PC2 (**G**) and PC2 versus PC3 (**H**). (**I–L**) Volcano plots displaying all expressed proteins filtered by fold change and p–value ($p < 0.01$, t–test).

Data are shown as mean ± SEM. For A, $n = 5–8$ per group; for B–C and E–F, $n = 3$ per group; and for D, $n = 4$ per group. p values were determined by one–way ANOVA with Tukey's multiple–comparisons test for A, D or unpaired two–tailed Student's t test for B–C and E–F. $^{**}P < 0.01$; $^{***}P < 0.001$; $^{****}P < 0.0001$; ns, not significant.

Supplemental Fig. 2. Protein–protein interaction network analysis of differentially expressed proteins following Mknk1 or Mknk2 perturbation.

BMDMs were transduced with lentivirus expressing control shRNA (shCtrl), shMknk1, or shMknk2, or with empty vector (EV) or Mknk2–overexpression lentivirus. Protein–protein interaction (PPI) networks were generated using STRING database interactions. Nodes represent individual proteins, and node size is proportional to the degree of connectivity within each network. Clusters are color–coded and functionally annotated based on GO biological process enrichment. **(A**) PPI network of proteins upregulated in both shCtrl vs. shMknk2 and shCtrl vs. shMknk1 comparisons. Twelve functional clusters were identified, including modules enriched for cell adhesion and migration/extracellular matrix organization (cluster 1), metabolic processes (clusters 2, 4, 6, 7, 8, and 9), mitochondrial respiration (clusters 5, 10, 11, and 12), and immune system processes (clusters 3 and 4). (**B**) PPI network of proteins downregulated in both shMknk2 and shMknk1 conditions. Six functional clusters were identified, dominated by metabolic processes (clusters 1–5) and cell cycle regulation (cluster 6). (**C**) PPI network of proteins uniquely upregulated in shMknk2 BMDMs. Four clusters were identified, all

associated with mitochondrial respiration and metabolic processes, with cluster 2 additionally enriched for immune and metabolic responses. (**D**) PPI network of proteins uniquely downregulated in shMknk2 BMDMs. Nine clusters were identified, spanning cell cycle and metabolic processes (cluster 1), metabolic processes and translation (clusters 2, 3, and 6), metabolic processes alone (clusters 4 and 5), RNA processing (cluster 7), protein transport (cluster 8), and cell adhesion and migration (cluster 9). (**E**) PPI network of proteins uniquely upregulated in shMknk1 BMDMs. Four clusters were identified, enriched for mitochondrial respiration and metabolic processes (cluster 1), and mitochondrial and cytoplasmic translation (clusters 2–4). (**F**) PPI network of proteins upregulated in MNK2–overexpressing BMDMs compared with EV control. A single cluster was identified, comprising integrin family members and exclusively enriched for cell adhesion and migration.

Supplemental Fig. S3. Flow cytometry gating strategy of T lymphocytes and NK cells in 4T1 tumors.

(**A)** Schematic of the experimental setup in which 4T1 mammary carcinoma cells were co–mingled in Matrigel with BMDMs transduced with control shRNA (shCtr), sh*Mknk1* or sh*Mknk2* lentiviruses (LVs), and injected subcutaneously into syngeneic mice. (**B–D**) Gating strategy for lymphoid cells, including assessment of activation and proliferation markers (**B**) and expression of immune checkpoint molecules (**C**) in CD4+ and $CD8^+$ T cells. (**C**) Gating strategy for NK cells based on CD49b and NKp46 expression and evaluation of their activation status.

Supplemental Fig. S4. Impact of *Mknk1* and *Mknk2* silencing in Mφs on T cell and NK cell activation.

(**A–D)** Flow cytometry analysis of inhibitory receptor expression on intratumoral $CD8^+$ T cells from shCtr-, sh*Mknk1*- or sh*Mknk2*-TAM co–mingling tumors: **(A)** LAG-3, **(B)** PD-1, **(C)** TIGIT and **(D)** TIM-3. **(E–I)** $CD4^+$ T cell cytotoxic function assessed by expression of GrzmB out of $CD4^+$ T cells (**E**) and out of $CD3^+$ T cells in (**F**); CD107a out of $CD4^+$ T cells in (**G**), and out of $CD3^+$ T cells in (**H**), and proliferation assessed by Ki–67 (**I**). **(J–M)** NK cell activation assessed by expression of IFN-γ in (**J**), GrzmB in (**K**), CD107a in (**L**) and perforin in (**M**).

Data are shown as mean ± SEM and presented as fold change relative to the shCtr group. For A, B and K, n = 23–24 mice per group; for C, n = 15–17 mice per group; for D and I, n = 8–10 mice per group; and for E–H, J and L–M, n = 30–32 mice per group. P values were determined by one–way ANOVA with Tukey's multiple–comparisons test. *$P < 0.05$; **$P < 0.01$; ns, not significant.

Supplemental Fig. S5. Flow cytometric characterization of intratumoral myeloid populations upon *Mknk1* or *Mknk2* silencing.

Flow cytometry analysis of myeloid cell populations in tumors from mice bearing shRNA–mediated knockdown of *Mknk1* (sh*Mknk1*) or *Mknk2* (sh*Mknk2*) compared to control (shCtr). Data are presented as fold change relative to shCtr. Total myeloid infiltration: (**A**) F4/80$^+$ TAMs, (**B**) CD11b$^+$ cells, **(C)** Ly6C$^+$ monocytes, (**D**) granulocytes, and (**E**) eosinophils all as a proportion of CD45$^+$ cells. TAM subset characterization: (**F**) Ly6C$^-$MHC II^{high} TAMs out of CD11b$^+$Ly6G$^-$ cells; (**G**) CD206$^+$F4/80$^+$ and (**H**) CD11c$^+$F4/80$^+$ cells within the F4/80$^+$ population. PD-1 expression on TAMs: (**I**) frequency of PD-1$^+$F4/80$^+$ cells within the F4/80$^+$ population and (**J**) MFI of PD-1 with F4/80$^+$ population.

Data are presented as mean values ± SEM and presented as fold change relative to the shCtr group. For A–G, *n* = 30–32 mice per group; for H;I, *n* = 15–17 mice per grou*p* values were determined by one–way ANOVA with Tukey's multiple–comparisons test. **P* < 0.05; ns = not significant.

Supplemental Fig. 6. Flow cytometry gating strategy of myeloid cells (**A**) Gating strategy for TAMs based on F4/80 expression and evaluation of immunostimulatory and immunosuppressive markers. (**B**) Gating strategy for CD11b$^+$ Ly6G$^-$ myeloid subpopulations.

S**upplementary Fig. 7. Effect of *Mknk2* overexpression in TAMs on intratumoral leukocyte populations.**

(A) Schematic of the experimental approach: BMDMs transduced with empty vector (EV), *Mknk1*- or *Mknk2*-lentivirus were co–injected with 4T1 mammary tumor cells subcutaneously into syngeneic mice. Tumors were harvested 9–10 days after injection for flow cytometric analysis. (**B–J**) Flow cytometry analysis of T cell and NK cell populations from dissociated 4T1 tumors, presented as fold change relative to EV. (**B**) CD4$^+$ T cell proliferation based on Ki–67 expression. (**C–F**) NK cell (NKp46$^+$CD49b$^+$) functional markers: (**C**) IFNγ, (**D**) GrzmB, (**E**) CD107a, and (**F**) Perforin. (**G–J**) Immune checkpoint receptor expression on CD8$^+$ T cells: (**G**) LAG-3, (**H**) PD-1, (**I**) TIGIT, and (**J**) TIM–3. (**K-X**) Flow cytometry analysis of myeloid cell populations, presented as fold change relative to EV. Frequencies of total myeloid populations out of CD45$^+$ cells: (**K**) CD11b$^+$, (**L**) F4/80$^+$ TAMs, (**M**) Ly6C$^+$ monocytes, (**N**) granulocytes, and (**O**) eosinophils. TAM subset characterization: (**P**) Ly6C$^+$ TAMs out of CD45$^+$; (**Q**) F4/80$^+$CD11c$^+$ out of F4/80$^+$; (**R**) CD206$^+$F4/80$^+$ out of F4/80$^+$; (**S**) CD80$^+$ and (**T**) CD86$^+$ on CD11b$^+$F4/80$^+$ cells; (**U**) MHC class II^{low} TAMs out of CD11b$^+$Ly6G$^-$. Immune checkpoint and inhibitory marker expression on F4/80$^+$ TAMs: (**V**) VISTA$^+$, (**W**) PDL–1$^+$, and (**X**) PD–1$^+$.

All data are presented as mean ± SEM and expressed as fold change relative to EV. Each data point represents an individual mouse. Statistical comparisons were performed by Mann–Whitney U test. *P < 0.05; ns, not significant.

Supplementary Fig. 8. Generation of shCtr and sh*Mknk2* hematopoietic chimeric mice and evaluation of immune cell populations in 4T1 tumors.
(**A**) Schematic of the experimental strategy in which hematopoietic stem and progenitor cells (HSPCs) were transduced with control shRNA (shCtr) or sh*Mknk2* lentivirus and transplanted into busulfan–conditioned recipient mice to generate hematopoietic chimeras. Following hematopoietic reconstitution, 4T1 mammary carcinoma cells were injected into the mammary fat pad of shCtr– and sh*Mknk2*–chimeric mice. (**B**) Mice were subcutaneously injected with 4T1 tumor cells. Tumor harvest and dissociation were performed 9 days after 4T1 cell inoculation. The flow cytometry analysis shows the proportions of different immune cell populations among $CD45^+$ cells from 4T1 tumors.

Supplemental Fig. 9. Expression patterns of canonical leukocyte, macrophage, monocyte, granulocyte and other immune cell markers across annotated clusters. (**A**) UMAP plot showing valid integration of the three different sequencing batches. (**B**) UMAP plots showing the expression of macrophage and myeloid granulocyte markers used for flow–cytometric sorting of Mφ) for scRNA–seq analysis. Ly6c identifies monocytes within the sorted macrophage population and reveals a distinct $Ly6c2^+$ population in macrophage cluster 2.
(**C**) Expression patterns in UMAP plots of $CD45^+$ leucocyte markers and major macrophage markers across clusters. (**D**) Expression patterns in UMAP plots of B cell (*Cd19*, *Cd79a*), dendritic cell (DC) (*Xcr1*, *Cd207*), mast cell (*Cpa3*, *Kit*), NK cell (*Ncr1*, *Gzmb*) and T cell (*Cd3e*, *Cd8a*) markers.

Supplemental Figure S1 related to Figure 1

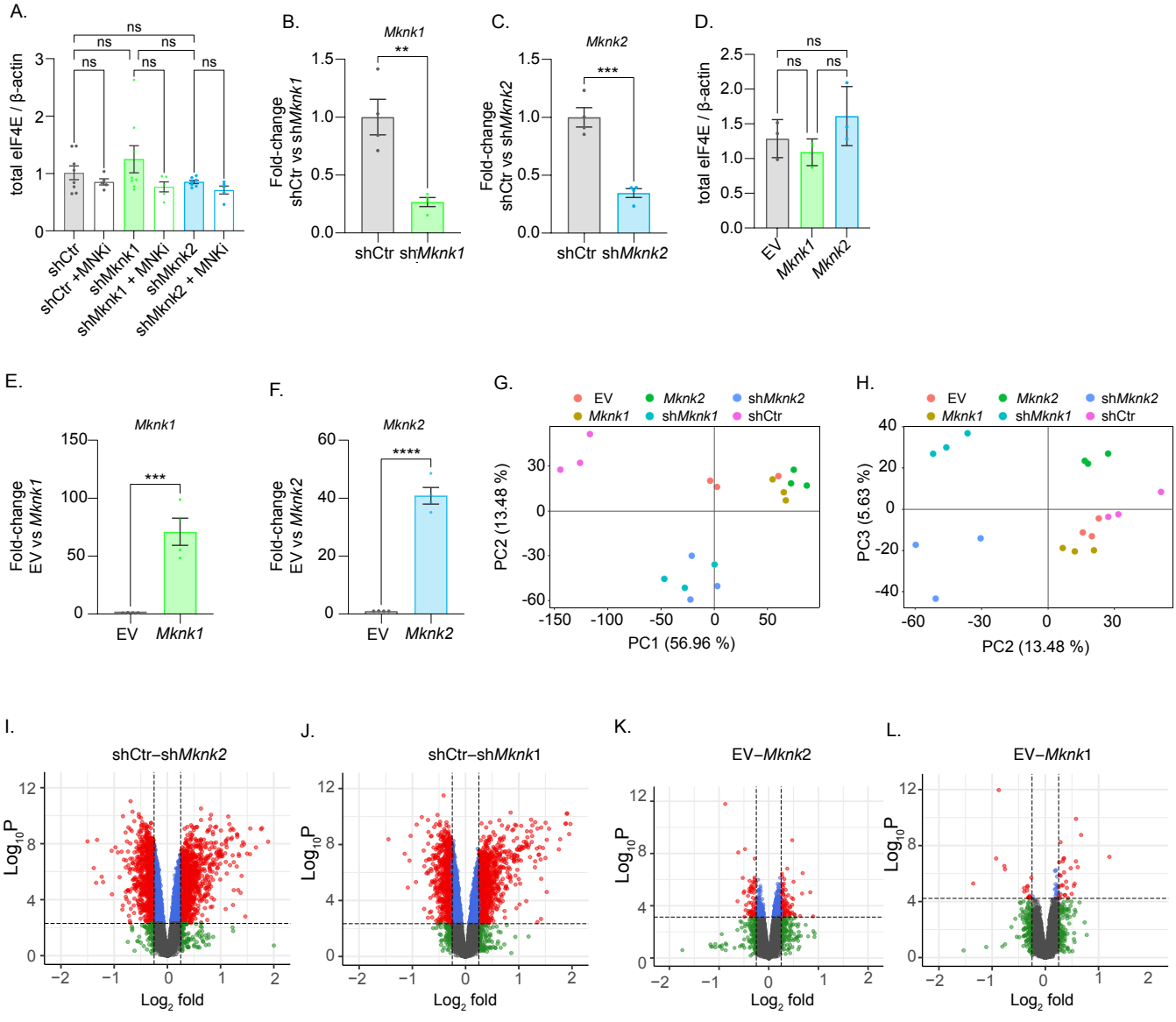

Supplemental Figure 2

A.

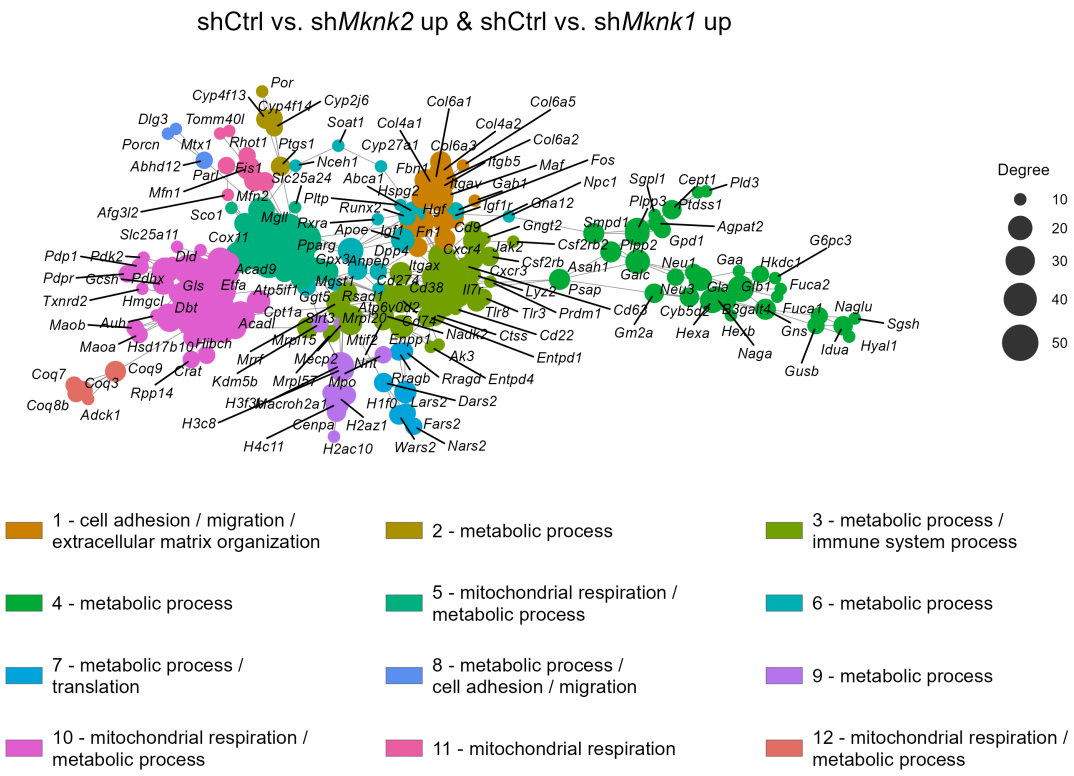

B.

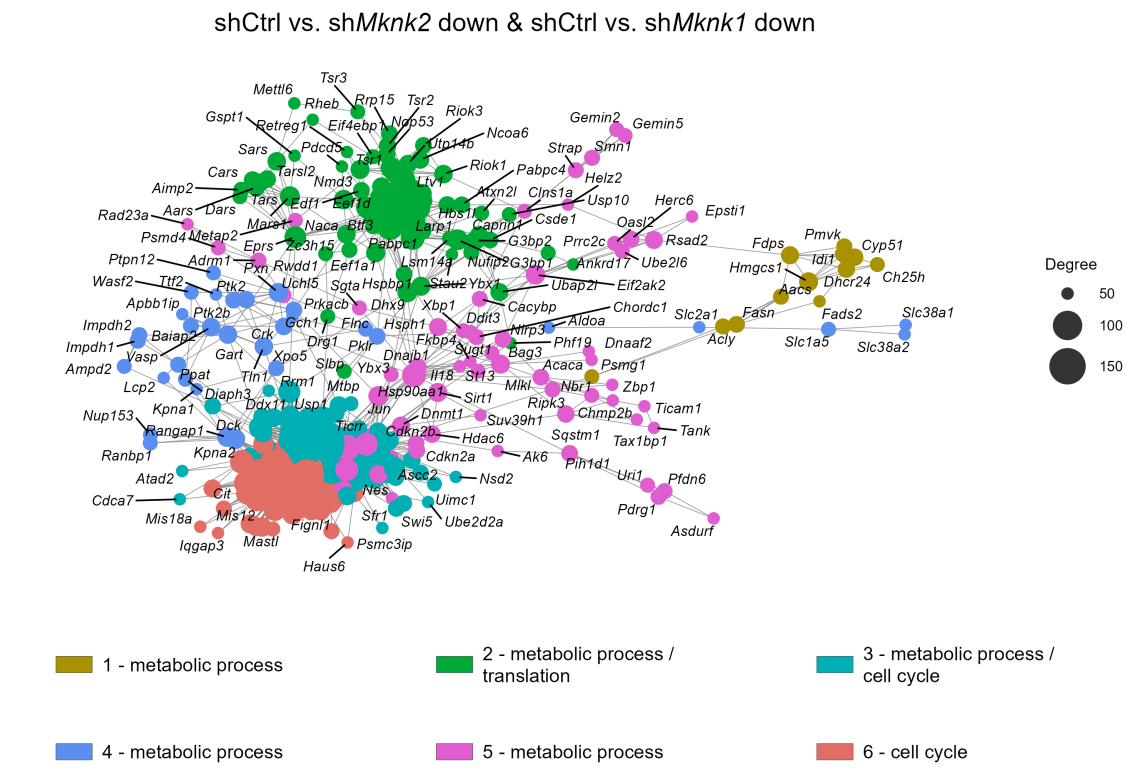

C

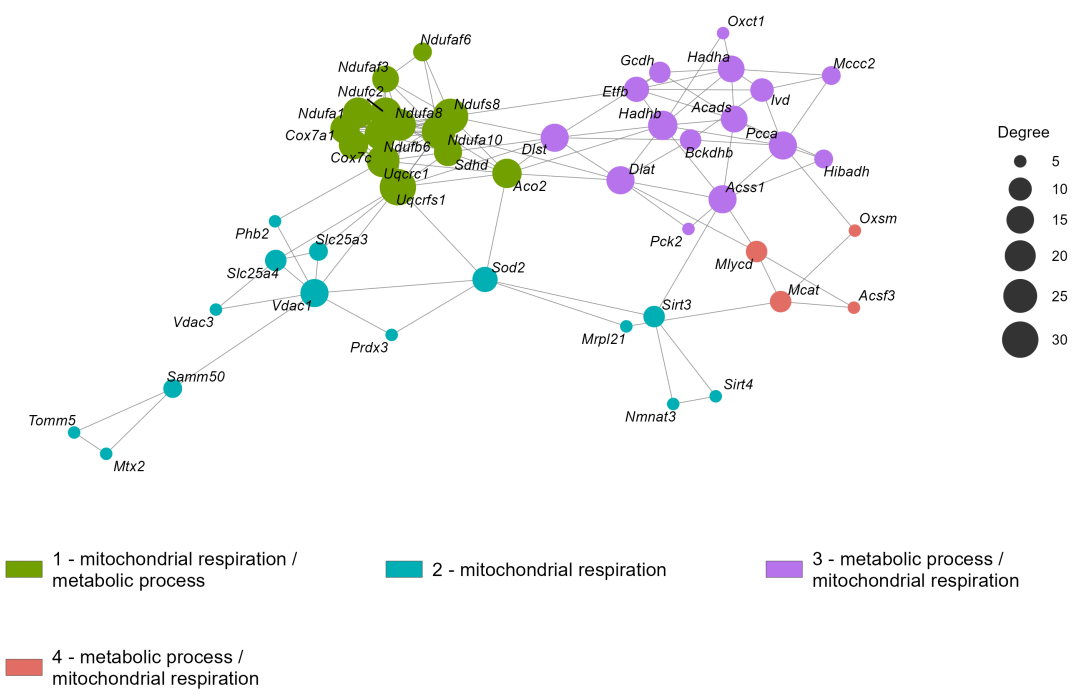

D

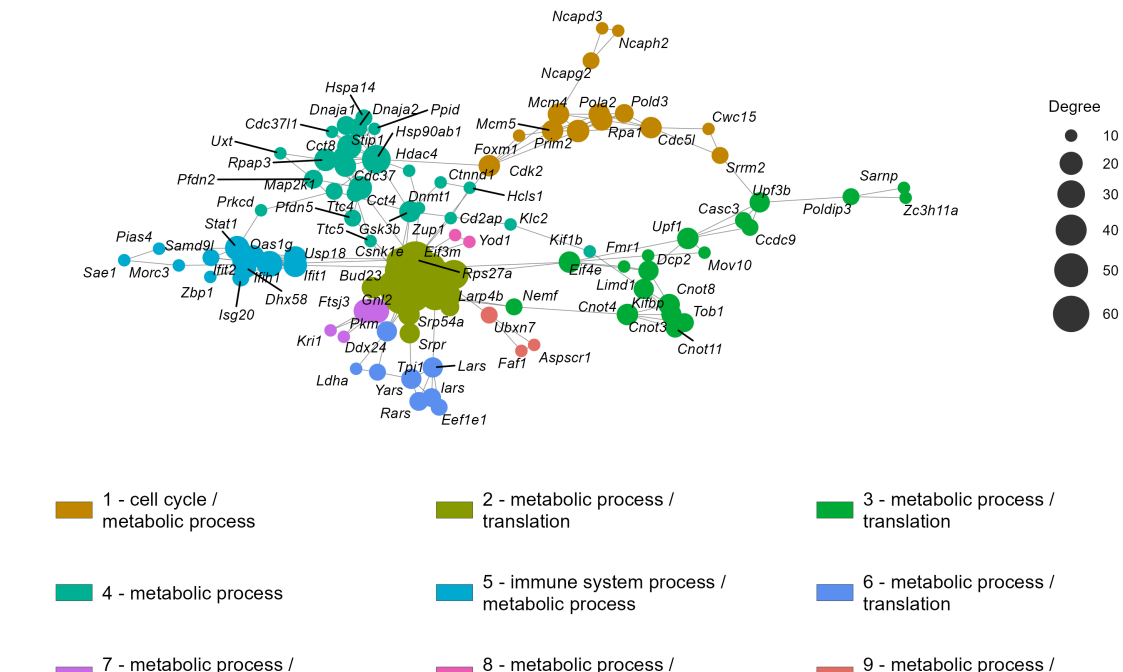

E

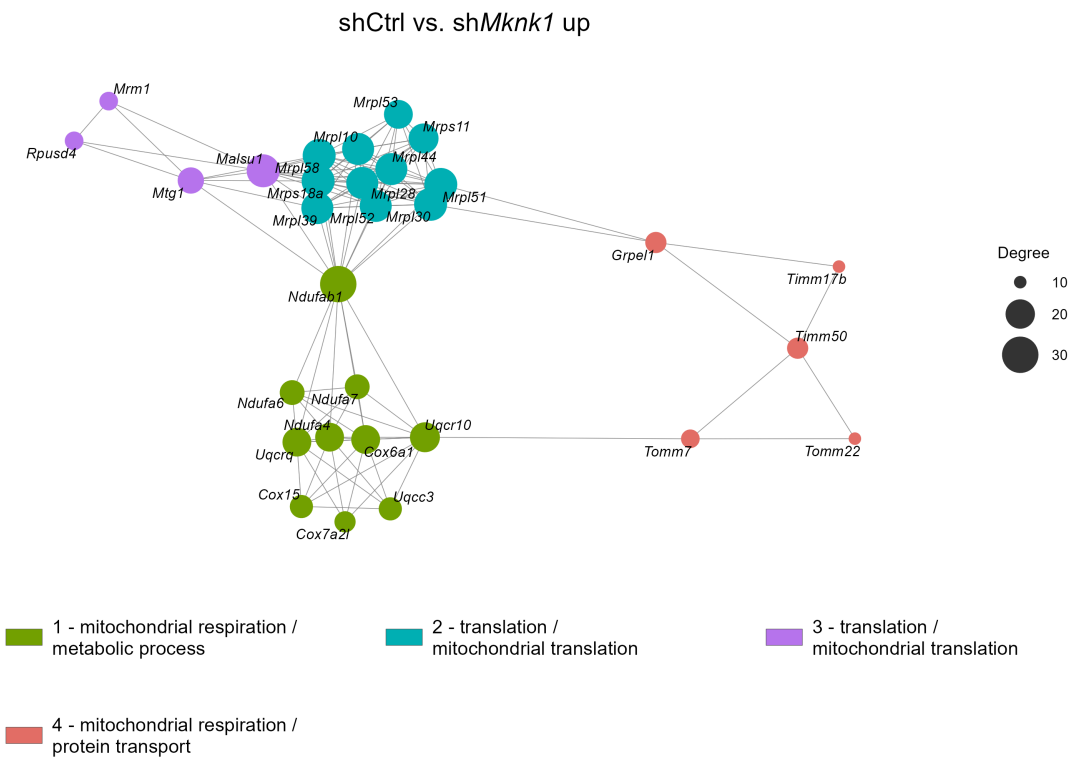

F

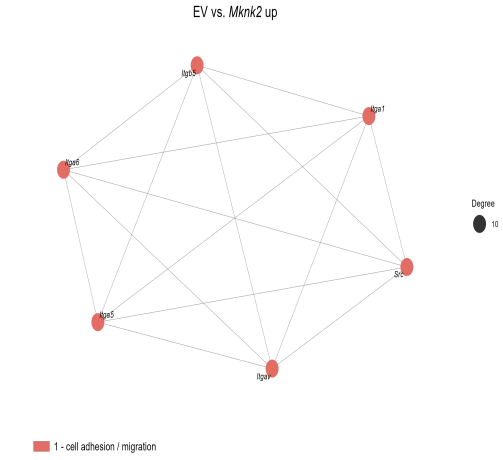

Supplementary Figure 3 related to figure 3

A.

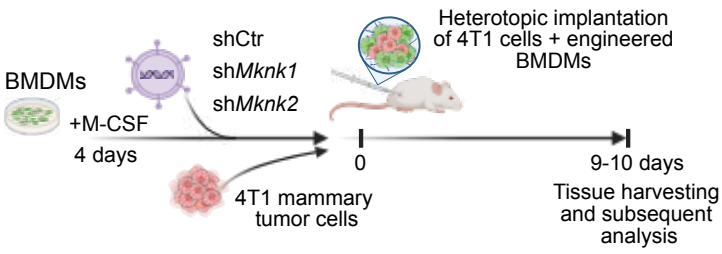

B.

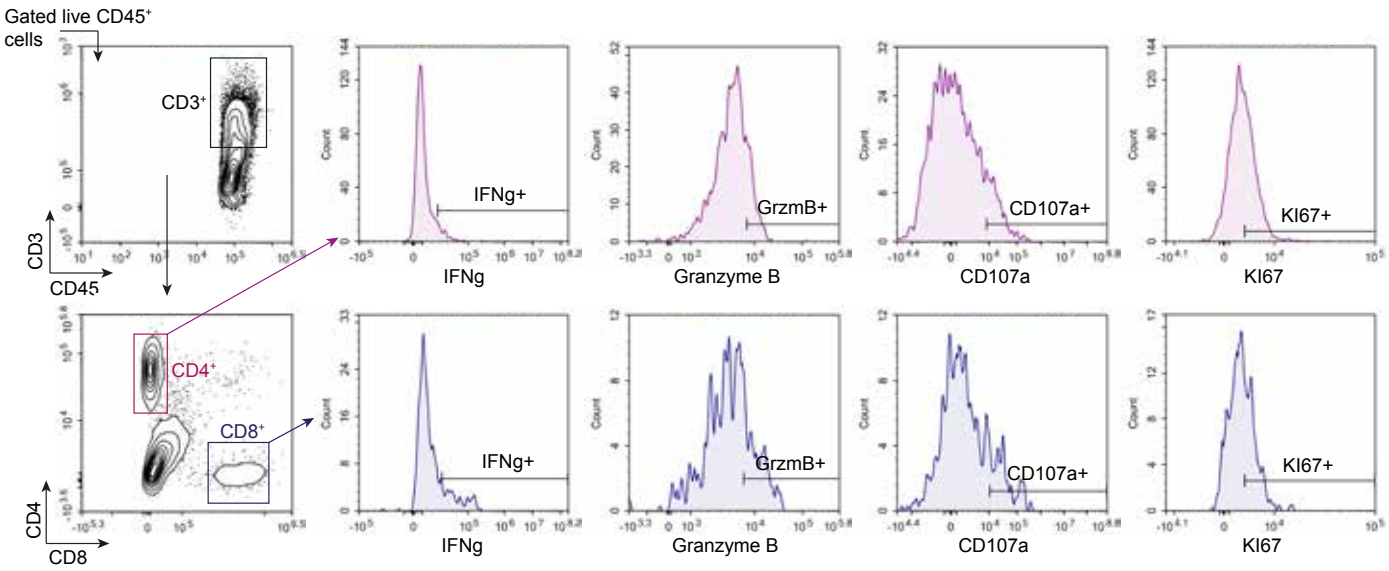

C

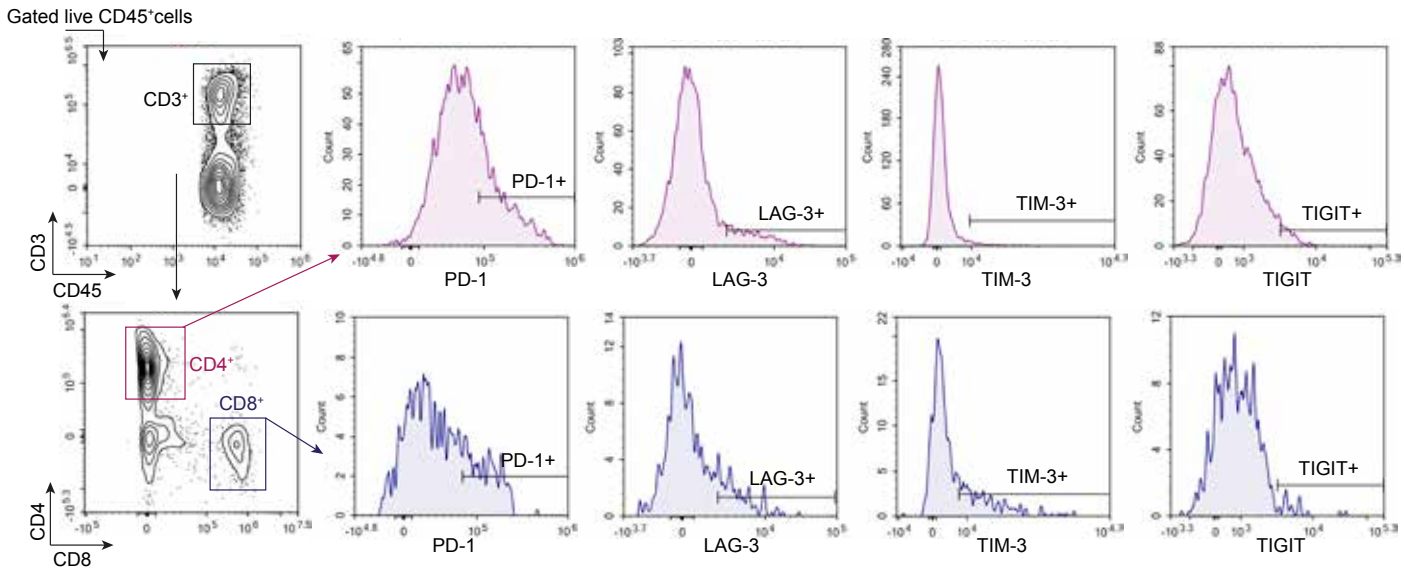

D.

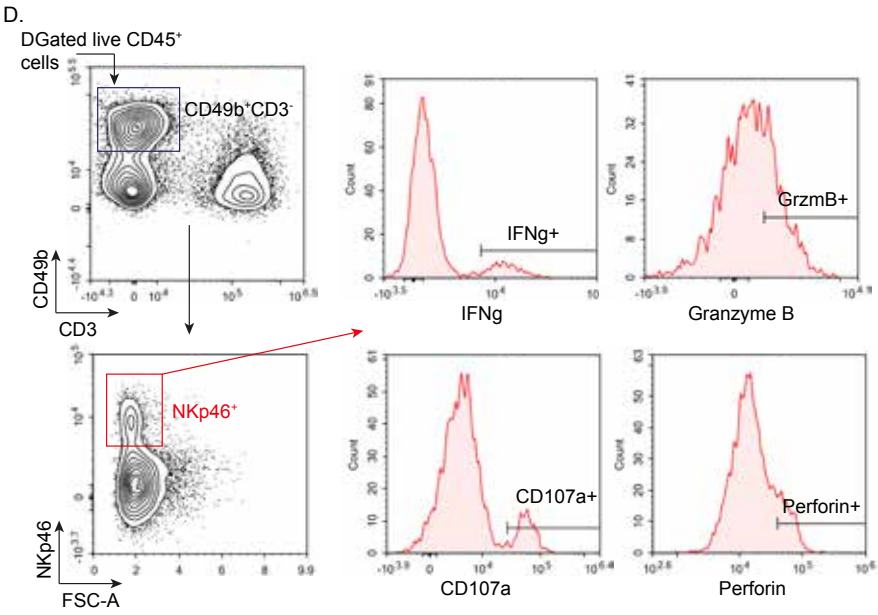

Supplemental Figure S4 related to Figure 2

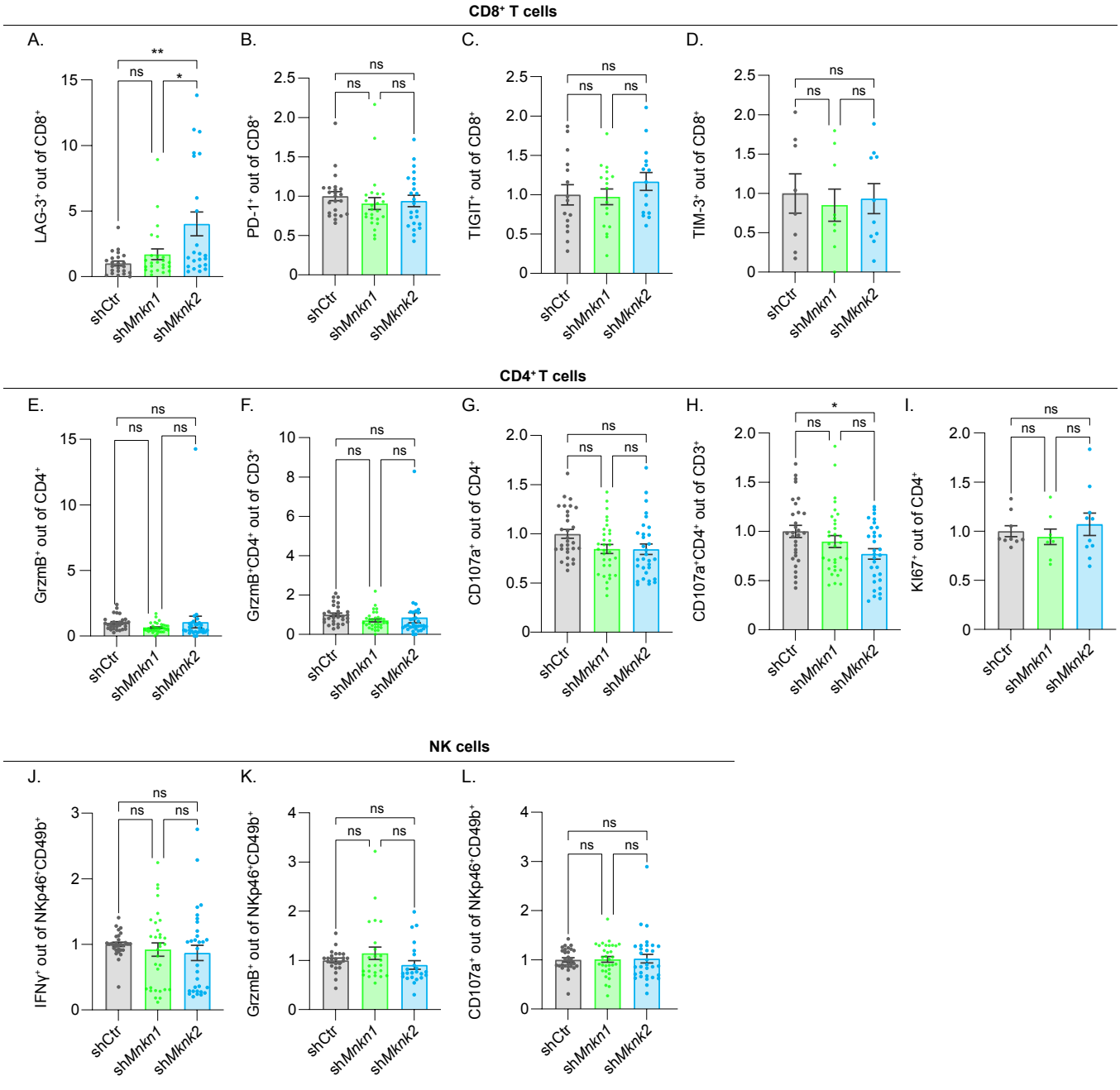

Supplemental Figure S5 related to Figure 4

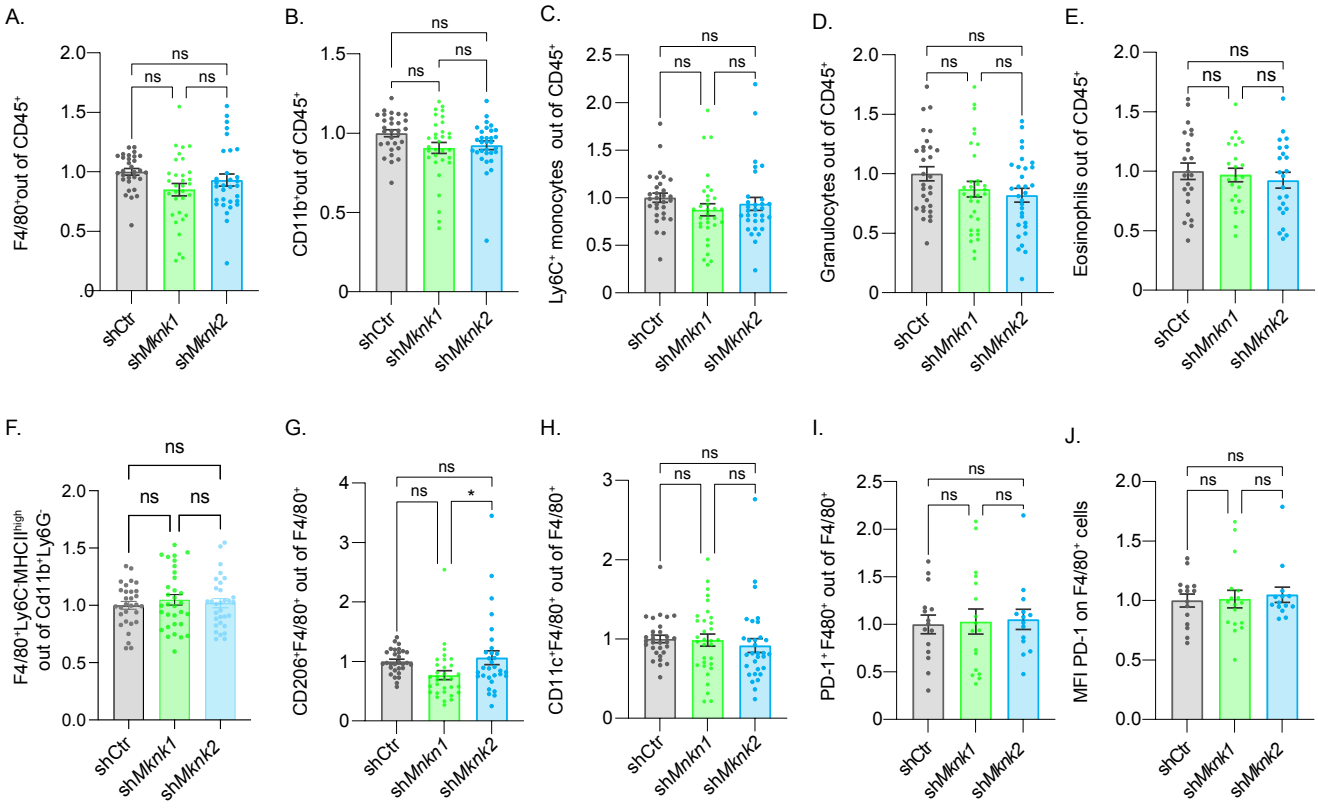

Supplementary Figure S6 related to Figure 3

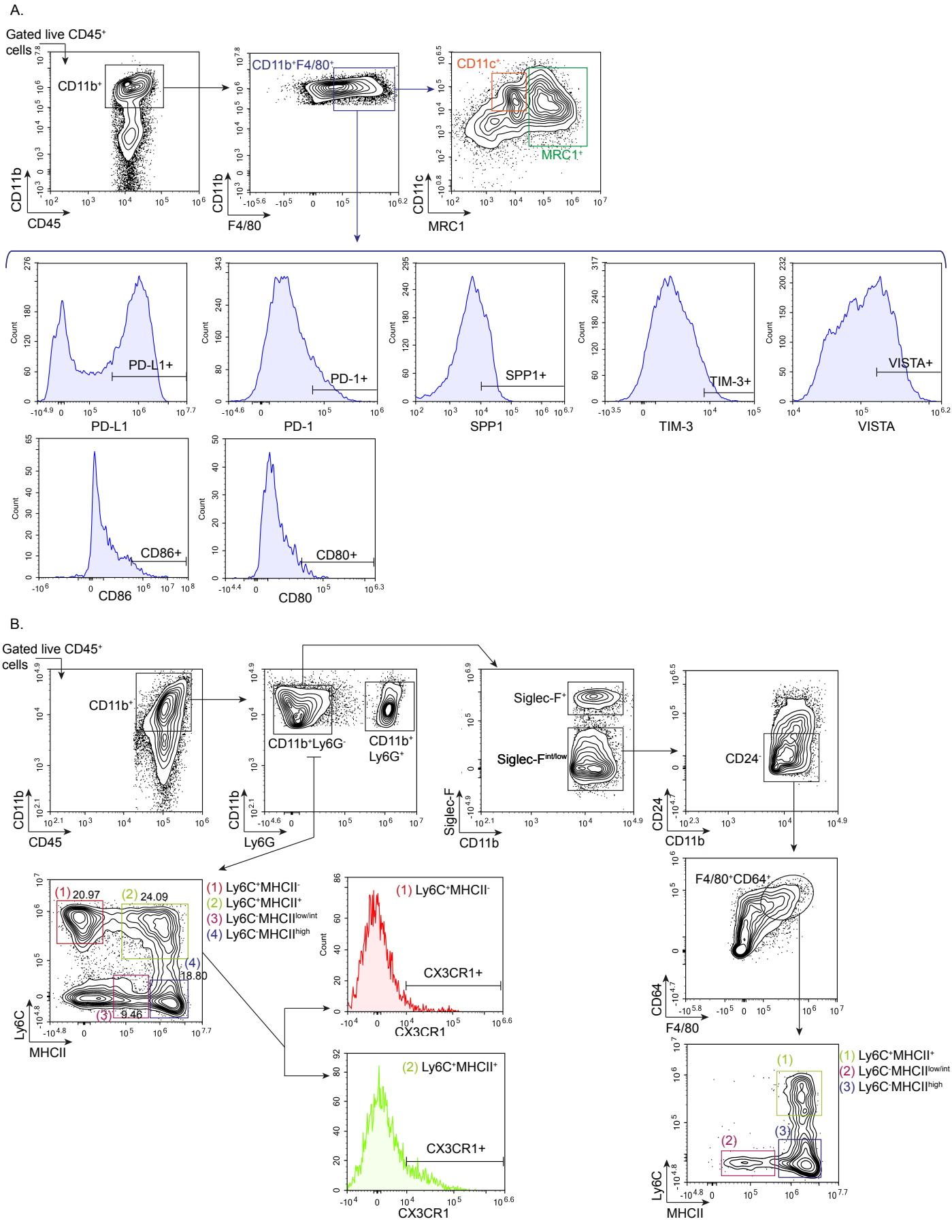

Supplemental Figure 7 related to Figure 4

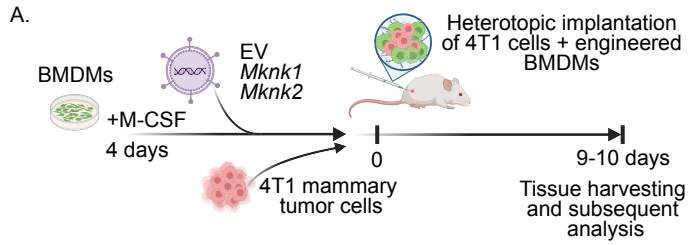

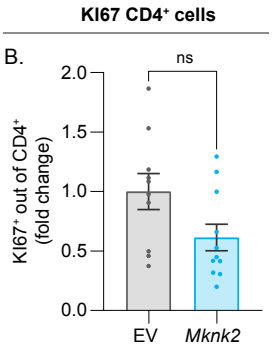

NK cells

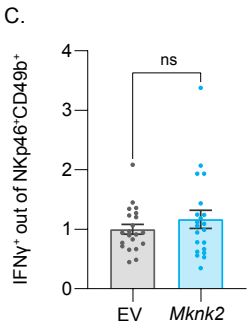

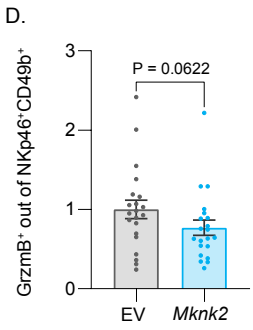

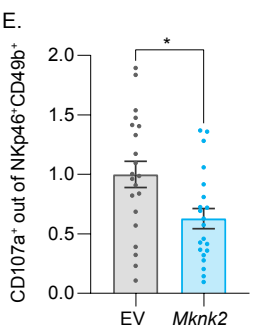

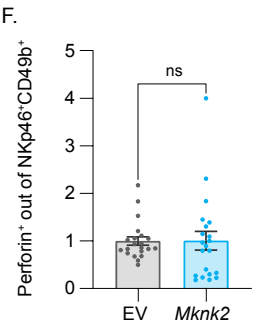

CD8⁺ T cells

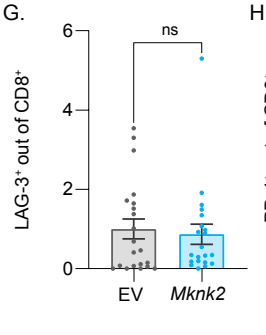

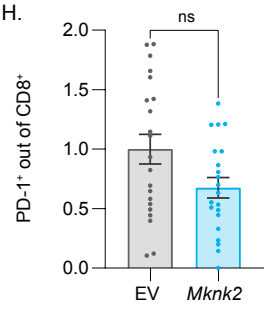

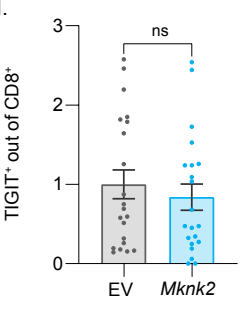

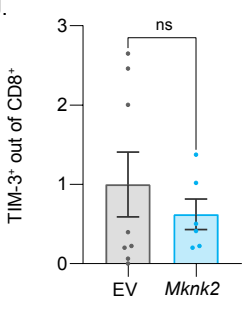

Myeloids cells

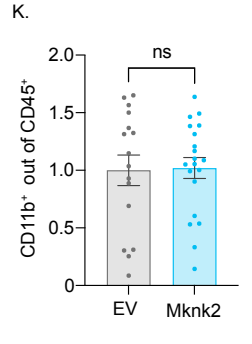

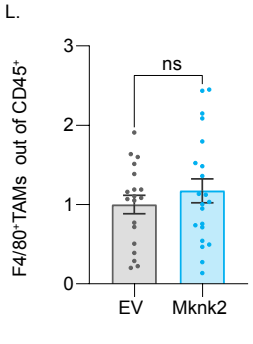

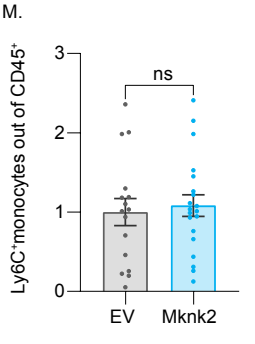

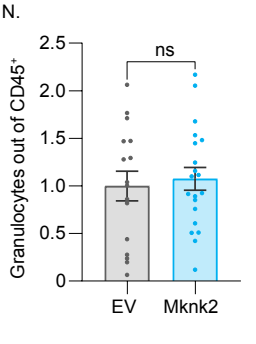

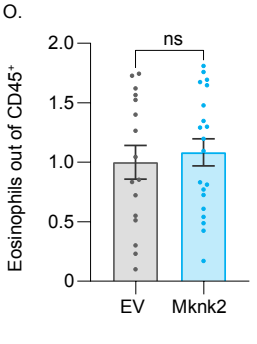

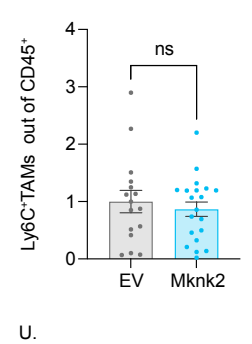

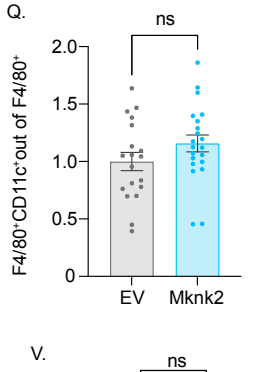

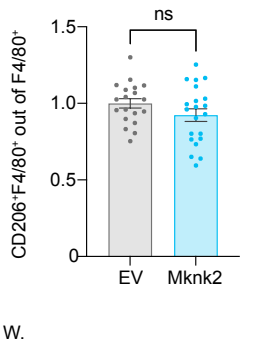

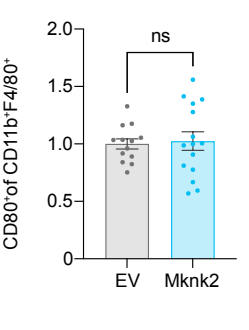

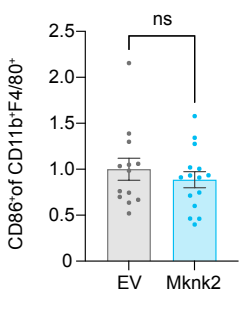

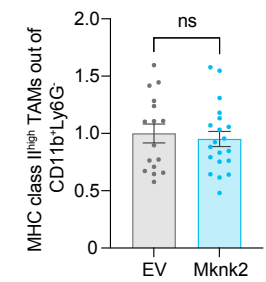

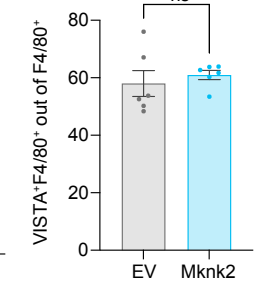

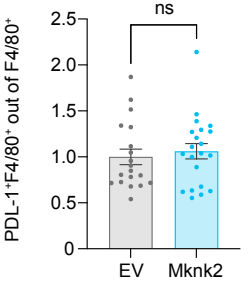

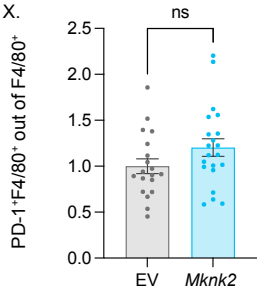

Supplemental Figure S8 realted to Figure 4

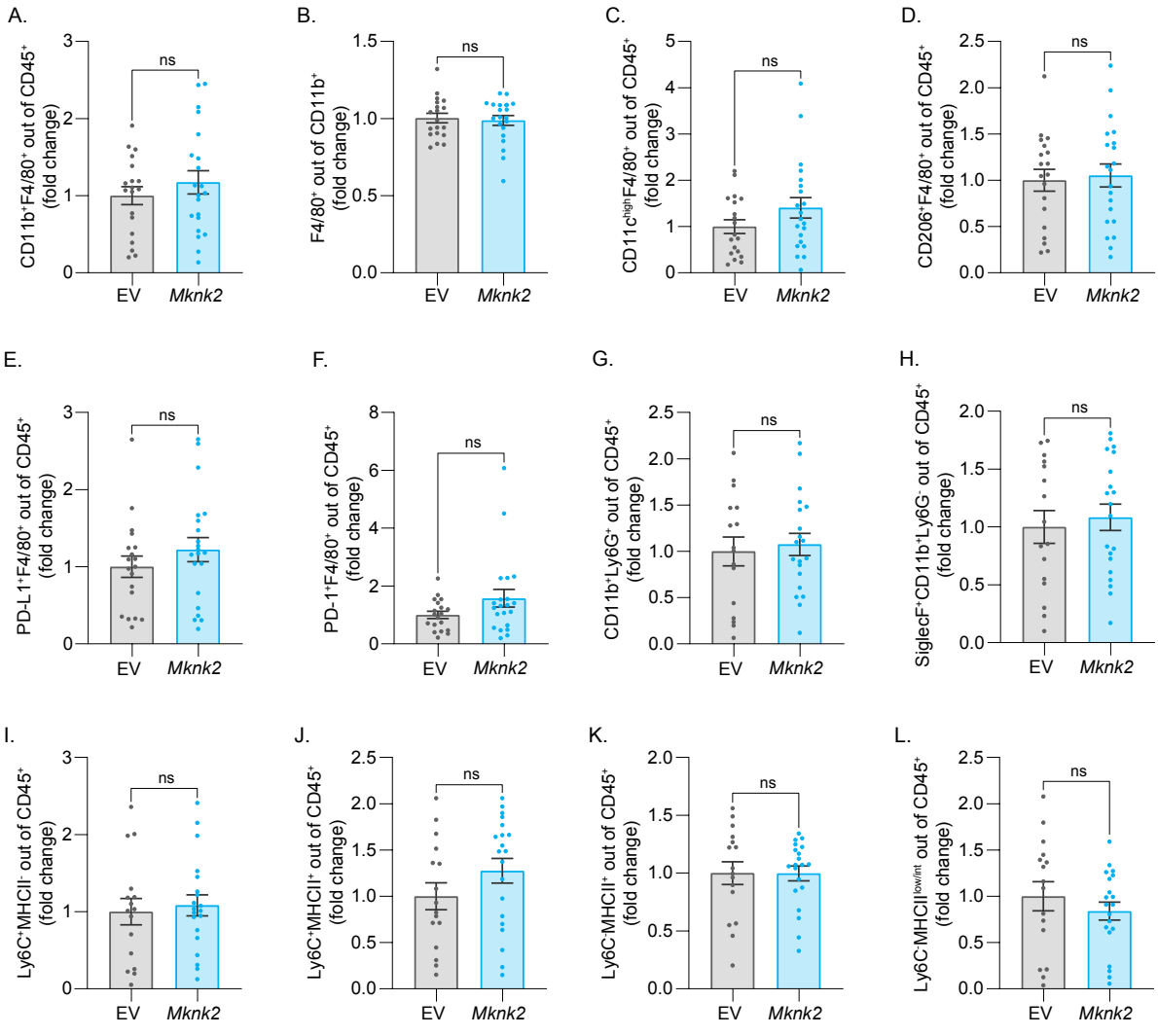

Supplemental Figure S10 related to Figure 6